J. Fluid Mech. (1999), *vol.* 397, *pp.* 1–22. Printed in the United Kingdom

Flow-induced instabilities of a mucus–serous bilayer

By J. A. MORIARTY† AND J. B. GROTBERG

Biomedical Engineering Department, University of Michigan, 3304 G. G. Brown Bldg, 2350 Hayward St., Ann Arbor, MI 48109-2125, USA

(Received 29 January 1996 and in revised form 25 March 1999)

In this paper we investigate the stability of a bilayer exposed to air flow. The bilayer consists of a viscoelastic solid layer (mucus), which rests on a viscous fluid film (serous fluid). The motivation behind this work is to examine the coupled, fluid/elastic instabilities related to mucus clearance in the lung where breathing and cough apply shear forces from the air flow onto the bilayer. Previous research on mucus transport due to air flow has not addressed the effects of the underlying serous layer nor those of surface tension at the mucus–air interface, two new features incorporated into the model. Surface tension effects are governed by the new parameter $\kappa' = (\sigma/dG')$ where σ is the air–mucus surface tension, G' is the elastic shear modulus of the mucus, and d is a characteristic thickness of the bilayer. The model predictions for the onset of unstable waves as a function of the parameters are compared to previous theories and experiments to provide physical interpretations and to compare results. The comparison with experiments show good qualitative and quantitative agreement. The results are compared, also, to flow over a single, viscoelastic layer, with no viscous fluid underneath, to demonstrate the appearance of new wave behaviour when the viscous fluid is added.

1. Introduction

Mucus clearance is an important process for normal pulmonary function providing, among other things, a cleansing mechanism for removing inhaled particles and micro-organisms. Clearance may occur by gravity drainage, ciliary motion, air flow shear forces and bi-phasic flow, all important aspects of pulmonary fluid dynamics as reviewed in Grotberg (1994). The latter two mechanisms are fluid/solid interactions which are similar in many ways to the stability studies of flows over compliant, viscoelastic coatings. There has been a great deal of work done in the past to examine the stability of compliant coatings when subjected to fluid flowing over them. The interest in studying such systems has typically been motivated by the desire to delay boundary layer transition, which has important ramifications in the design of surfaces for enhanced drag reduction; airplane wings and yacht hulls are just two examples of problems which would utilize this technology. The reader is referred to Riley, Gad-el-Hak & Metcalfe (1988) for a comprehensive review article on this topic.

† Current address: Baxter Healthcare Inc., Route 120 & Wilson Rds., Round Lake, IL 60073, USA.

Mucus is a viscoelastic material. The components of mucus which provide its viscoelastic properties are glycoproteins, often referred to as mucins. These mucins are extended rods, normally 500–900 nm long and 10 nm wide, which are cross-linked into a three-dimensional network by disulphide bonds (Wu & Carlson 1991). They are released from mucous goblet and gland cells as droplets 1–2 μm in diameter, which then rapidly swell by a factor of several hundred through absorption of water from the underlying serous fluid layer. They spread out under the action of cilia on the serous layer surface to form sheets, which are then, under normal conditions, carried along above the serous layer by the action of the cilia (Sleigh, Blake & Liron 1988). The mucus layer exists from the trachea outward to approximately airway generation 15 or so. Because mucus is composed of a watery serous solution bound within a matrix of cross-linked mucins, the serous molecules on the air/mucus surface give rise to an interfacial tension there. Schurch *et al.* (1990) have measured this interfacial tension to be 32 dyn cm^{-1}.

In addition to viscoelasticity, mucus exhibits non-Newtonian behaviour including a finite yield stress ($\sim$ 500–600 dyn cm^{-2}), shear-thinning and thixotropy. It has a frequency-dependent shear modulus which increases to a plateau as frequency increases, the asymptote ranging over an interval $G' \sim$ 30–300 dyn cm^{-2}, depending on the measurement techniques and condition of the mucus, see Dulfano, Adler & Philippoff (1971), Davis (1973), Powell *et al.* (1974) and King & Macklem (1977). The mucus layer is typically thin (5–10 microns in healthy humans); however, in the case of disease this thickness could be many more times greater than normal. Lung pathology may also change the material properties of the mucus. Cystic fibrosis, for example, causes mucus to become much more viscous and elastic, owing in part to interlinking of DNA strands from cellular and bacterial debris. This additional structure to the mucus complex inhibits mucus clearance, a major clinical problem in cystic fibrosis. Treatments aimed at breaking down the DNA, and reducing the viscosity and elasticity, show promise (Shah *et al.* 1996). The mucus lining covers a thin viscous sublayer, the serous layer, which is a watery-type solution covering the ciliated bronchial epithelium. The serous layer is typically 5–10 μm in healthy humans but may vary with the state of hydration within the lung as well during disease. Most authorities view the serous fluid as Newtonian. The total bilayer thickness to airway radius ratio, $\theta \sim O(10^{-3}$–$10^{-2})$ for healthy lungs and $\theta \sim O(10^{-1}$–$1)$ for certain diseases such as chronic bronchitis and cystic fibrosis. In severe asthma, for example, mucus plugging of small airways may occur where $\theta \to 1$.

Airways tend to be aerodynamically short, i.e. the entrance lengths for developing flow are longer than the tube lengths. Also, the largest airways experience turbulent air flow as has been modelled by Basser, McMahon & Griffith (1989), Clarke, Jones & Oliver (1970), and King, Chang & Weber (1982). The air flow over the mucus may cause unstable waves on its surface, if the flow rate is sufficiently large. These instabilities grow, and may eventually shear off into minute droplets forming a biphasic flow which removes mucus very efficiently. Air speeds are particularly high during cough, $\sim$ 200 m s^{-1} according to Ross, Gramiak & Rahn (1955), which are of similar magnitude to the elastic wave speed of the trachea, for example, 80–120 m s^{-1} (Suki *et al.* 1995). Consequently, in the lung, instabilities of the mucus layer may be desirable since they can increase the effectiveness of cough (King *et al.* 1982).

Recently, Evrensel *et al.* (1993) adapted the analysis of flow over compliant coatings to look specifically at the problem of mucus clearance in the lung. Their system is one of steady air flow passing through a cylindrical tube coated with a viscoelastic

layer. The coating is anchored at its interface with the underlying tube wall, there being no serous sublayer as may occur in severe dehydration. The base state is taken to be fully developed, Poiseuille flow in the tube. Assuming small-amplitude perturbations to the base state, Evrensel *et al.* (1993) conduct a linear stability analysis which leads to solution of the relevant Orr–Sommerfeld equation coupled to the solid stress field at the air/mucus interface. Their analysis pertains to a single layer whose thickness/radius ratio falls in the range $0.1 < \theta < 0.6$. They find that the critical flow speed which precipitates instabilities decreases with increasing mucus thickness. This is consistent with the findings of Clarke *et al.* (1970), whose coated tube experiments were for $0.06 < \theta < 0.24$ and whose critical air flows were turbulent, $3000 < R_e < 10\,000$.

There have also been many experimental studies conducted to study the effectiveness of cough. King *et al.* (1982) carried out experimental work on both steady and oscillatory air flow over mucus simulants (locust bean gum or hog gastric mucin) coating the inner surface of a tube. In the steady air flow experiments, it was found that varying the thickness of the mucus layer in the range $0.01 < \theta < 0.05$ caused no systematic effect on the critical air velocity required for unstable wave production. A later paper, King, Brock & Lundell (1985), examined the relationship of the simulated mucus layer thickness and rheology with its clearance by simulated cough, created by sudden opening of a pressurized air tank into the test section. Peak Reynolds numbers for this transient pulse (duration ~ 0.5 s) of air flow fall in the range $\sim 15\,000 < R_e < 35\,000$. By injecting tracer particles on to the surface of the compliant layer, they examined particle clearance, and observed that particle movement was caused by the crests of waves pushing the particles along. Hence they surmised that particle clearance and wave formation are related phenomena. Their results indicate that clearance rate is influenced by mucus viscoelasticity and mucus layer thickness; thicker layers resulted in greater clearance. A similar apparatus was used by Scherer & Burtz (1978) for flow over purely viscous fluid layers.

Basser *et al.* (1989) conducted experiments on flow over a mucus simulant (mayonnaise) in a rectangular channel. They hypothesize that an 'avalanche' phenomenon is responsible for mucus clearance in the lung. The instability of the air/mayonnaise interface is seeded when a region of mayonnaise on the floor of the channel reaches its yield stress and starts to flow locally. This local movement leads to a piling and thickening of the mayonnaise resulting in crest formation at the mayonnaise/air interface. Air flowing over the crest has increased velocity, and this entails larger stresses which can lead to yielding in a region local to the surface of the crest. The region of yielding grows until some portion of the mayonnaise makes contact with the top of the channel, thereby blocking air flow, and precipitating a catastrophic clearance event. Their turbulent critical air flows had a Reynolds number range, $2000 < R_e < 16\,000$.

Duncan, Waxman & Tulin (1985), in their work on flow over compliant surfaces, considered a system of inviscid fluid flow (modified by pressure amplitude and phase shifts to simulate boundary layer phenomena) over a two-dimensional viscoelastic Kelvin–Voigt solid, resting on a rigid flat boundary. Their parameter choices were confined to a fluid/solid density ratio of unity, appropriate for liquid flows over compliant coatings, unlike the airway system where this ratio is $O(10^{-3})$. Assuming small sinusoidal disturbances they conducted a linear stability analysis for the system to determine how the onset flow speed and growth rate of instabilities depend on different system parameters. They then explained their results in terms of the energy classification arguments derived by Landahl (1962) and Benjamin (1963).

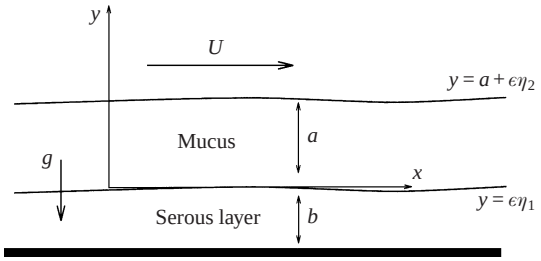

FIGURE 1. Schematic of the air/mucus layer/serous layer system.

In the present work, we consider a system in which air flows over a viscoelastic solid lying on top of a viscous sublayer. In addition, our model considers the effect of surface tension at the air/mucus interface. Neither of these features have been studied by previous investigators. By assuming small sinusoidal disturbances we conduct a linear stability analysis of the system. Since the mucus and serous layers are thin with respect to the airway tube radius, i.e. $\theta \ll 1$, we assume channel flow for a planar geometry. In the limit that the thickness of the viscous sublayer tends to zero, and there is no surface tension acting at the air/mucus interface, we recover the dispersion relationship derived by Duncan *et al.* (1985), which is a less complicated function of the complex wave speed c and the disturbance wavenumber k. We also use the wave classification arguments of Landahl (1962) and Benjamin (1963) to elucidate the fundamental nature of the air/solid/fluid interaction and its instabilities.

2. Mathematical model

2.1. *Assumptions and scaling*

A mucus slab, of thickness a, lies on a serous layer of thickness b. These are both small compared to the radius of the airway tube, and hence we assume the velocity and displacement fields in the serous and mucus layers are both locally planar. There is an air flow of magnitude U_∞ over the mucus which simulates the air flow generated during breathing. The mucus/air and serous/mucus interfaces are given by $a + \epsilon\eta_2$ and $\epsilon\eta_1$ respectively, where η_1 and η_2 represent deviations from flat surfaces. Surface tension σ acts at the air/mucus interface, and gravity g acts downwards towards the airway wall. The airway tube is assumed to be much less compliant than the mucus, and hence we treat it as rigid. The basic model is illustrated in figure 1.

Since the stress levels imparted to the mucus are below the mucus yield stress, we model the mucus as a viscoelastic solid with storage modulus (elastic shear modulus) G', dynamic loss modulus (viscous modulus) G'' and density ρ_m. This assumption is justified later, when we calculate the stress in the mucus at the onset of instability, and verify that it is indeed below that of the yield stress. The serous layer is treated as a Newtonian fluid with constant viscosity, μ_s, and density, ρ_s.

The displacements in the mucus are denoted $\boldsymbol{U}_m = (U_m, V_m)$ and the serous velocities are denoted $u_s = (u_s, v_s)$. We scale $x, y, U_m, V_m \sim b$, and $u_s, v_s, U_\infty \sim C_t$, the transverse wave speed in an ideal elastic solid; $C_t = (G'/\rho_m)^{1/2} = 5.62\,\mathrm{cm\,s^{-1}}$ for mucus Powell *et al.* (1974); and the pressure $p \sim \mu_s C_t/b$. The dimensionless mucus thickness and air flow speed are then $\hat{a} = a/b$ and $\hat{U} = U_\infty/C_t$, respectively, where the hat signifies a dimensionless quantity. Time, t, is scaled on b/C_t. The variables which appear in the following equations are the dimensionless forms.

With this scaling, the dimensionless stress tensor for the viscoelastic solid σ_{ij}^m is given by

$$\sigma_{ij}^m = \left(\frac{1}{G_\lambda} - 2(1+\mathrm{i}\delta)\right)\delta_{ij}U_{m_{kk}} + (1-\mathrm{i}\delta)\left[\frac{\partial U_{m_i}}{\partial x_j} + \frac{\partial U_{m_j}}{\partial x_i}\right], \tag{1}$$

where $G_\lambda = C_t^2/C_1^2$, δ_{ij} is the Kronecker delta and δ is a measure of the viscous damping in the mucus, $\delta = G'/G''$. Note that $\delta = 0$ is the purely elastic limit for the mucus layer and that the complex form of the viscous damping in (1) anticipates travelling wave solutions which, eventually, will be expressed in complex form. In the present work, we shall assume a Kelvin–Voigt model for the viscoelastic material, so that δ is linearly proportional to the frequency of the motion. We assume there is no damping in the longitudinal direction, and thus the longitudinal wave speed C_L is the same as that in the elastic solid $C_l = (E/\rho_m)^{1/2}$ where E is Young's modulus. Similarly, the dimensionless stress tensor for the viscous fluid σ_{ij}^s is given by

$$\sigma_{ij}^s = \gamma\left[-p\delta_{ij} + \frac{\partial u_i}{\partial x_j} + \frac{\partial u_j}{\partial x_i}\right], \tag{2}$$

where $\gamma = \mu_s/\rho_m b C_t$ is the ratio of the serous layer to the mucus shear stress.

2.2. *Governing equations*

The governing equation for the displacement field in the mucus layer, with gravity acting in the negative y-direction is then,

$$\frac{\partial^2 \boldsymbol{U}_m}{\partial t^2} = (1+\mathrm{i}\delta)\nabla^2\boldsymbol{U}_m + \left(\frac{1}{G_\gamma} - (1-\mathrm{i}\delta)\right)\nabla(\nabla\cdot\boldsymbol{U}_m) - \boldsymbol{G}\boldsymbol{j}, \tag{3}$$

where $G = gb/C_t^2$. We assume that the serous layer behaves as a Newtonian fluid, and that the Reynolds number of the flow in the serous layer is much less than unity so that Stokes flow applies. Thus, the governing equation for the velocity field in the serous layer is

$$\nabla^2\boldsymbol{u}_s - \frac{GR_s}{\gamma}\boldsymbol{j} = \nabla p_s, \quad \nabla\cdot\boldsymbol{u}_s = 0, \tag{4}$$

where $\boldsymbol{u}_s = (u_s, v_s)$ is the velocity in the serous layer, p_s is the pressure and $R_s = \rho_s/\rho_m$.

For the air flow, we assume a simplified model which incorporates both the viscous and inviscid effects of the flow. We decouple these effects, such that the viscous component of the air flow is turbulent boundary layer flow over the mucus in its unperturbed state and the inviscid component is due to the presence of the wavy boundary. This is a reasonable approximation considering $\mu_a/\mu_s \ll 1$, where μ_a is the viscosity of the air, and hence the viscous effects of the perturbed air flow will be small compared to the viscous effects of the perturbed serous layer flow field.

The inviscid component is determined using potential flow theory for flow over a small-amplitude wavy boundary. Thus if the wavy boundary has wavenumber, k, and complex wave speed, c, then $\boldsymbol{u}_a = \hat{U}\boldsymbol{i} + \epsilon\nabla\Phi$, where

$$\Phi = -\mathrm{i}[\hat{U} - c]\mathrm{e}^{-k(y-\hat{a})}\eta_2. \tag{5}$$

In this case, ϵ is the amplitude of the perturbation relative to the serous layer thickness. For this potential flow field, the pressure due to the wavy boundary is then

$$p_{a1} = -\mathrm{e}^{-k(y-\hat{a})}\frac{R}{\gamma}[\hat{U} - c]^2 k\eta_2, \tag{6}$$

where $R = \rho_a/\rho_m$ is the ratio of air to mucus densities.

Quantities	Magnitude	Dimensionless parameters	Magnitude
Mucus depth, a	$\sim 50\,\mu$m	$\hat{a}$	1
Serous layer depth, b	$\sim 50\,\mu$m		
Air density, ρ_a	10^{-3} g cm^{-3}	$R = \rho_a/\rho_m$	0.001
Serous layer density, ρ_s	1 g cm^{-3}	$R_s = \rho_s/\rho_m$	1
Mucus density, ρ_m	1 g cm^{-3}		
Transverse elastic wave speed, C_t	5.62 cm s^{-1}	$G_\lambda = C_t^2/C_l^2$	0.0909
Longitudinal elastic wave speed, C_l	18.61 cm s^{-1}		
Complex loss modulus, G''		$\delta = G''/G'$	
Flow speed, U_∞		$\hat{U} = U_\infty/C_t$	
Serous viscosity, μ_s	0.017 P	$\gamma = \mu_s/\rho_m C_t b$	0.605
Gravity, g	981 cm s^{-2}	$G = gb/C_t^2$	0.158
Surface tension, σ	10 dyn cm^{-1}	$\kappa = \sigma/bG'$	62.3

TABLE 1. Parameters used for the air–mucus–serous system.

2.3. *Boundary conditions*

At the mucus/air interface we impose continuity of normal and tangential stresses. The normal stress condition requires that $[\sigma_{ij} n_i n_j] = \kappa n_{i,i}$, where σ_{ij} is the stress tensor of either the air or viscoelastic media, n_i is the unit normal of the surface $(-\epsilon\eta_{2x}, 1)/(1 + (\epsilon\eta_{2x})^2)^{1/2}$, [ ] refers to a 'jump' and $\kappa = \sigma/bG'$ is the dimensionless surface tension at the air/mucus interface. Similarly, continuity of tangential stress requires that $[\sigma_{ij} n_j t_i] = 0$. Since we assume the air flow has a base-state viscous component, and an inviscid first-order component, the viscous components in the stress balances at the mucus/air interfaces only come into leading order. We also impose the kinematic condition at this interface, but not continuity of tangential velocity. At the serous/mucus interface, continuity of normal and tangential stress is imposed, as well as the kinematic condition in both the mucus and the serous layers. The no-slip condition, $[u_i t_i] = 0$, is also imposed at this interface. Finally, at the boundary $y = -1$, we impose conditions of no slip and no penetration. These conditions are written out explicitly for the first-order problem, § 3.2. The dimensionless parameters, therefore, arising in the problem are: $\gamma, R, R_s, \delta, G_\lambda, \kappa, G, \hat{a}$ and $\hat{U}$. Values of these parameters of the air–mucus–serous system are given in table 1.

3. Problem solution

We seek solutions by expanding in terms of the small-amplitude parameter ϵ, so that $\boldsymbol{u} = \boldsymbol{u}_{s0} + \epsilon \boldsymbol{u}_{s1}$, $\boldsymbol{U}_m = \boldsymbol{U}_{m0} + \epsilon \boldsymbol{U}_{m1}, p_s = p_{s0} + \epsilon p_{s1}$.

3.1. *Leading-order problem*

In the leading-order problem the air flow imparts a shear stress to the mucus, thus dragging it at constant velocity τ/γ, where τ is given by Schlichting (1979),

$\tau = (0.0288)R\,\hat{U}^2\ R_e^{-1/5}$, and R_e is the Reynolds number of the air flow. Typically $R_e \sim O(2000\text{–}4000)$ in the largest airways like the trachea and major bronchi, so that the turbulent boundary layer assumption is valid over most of the range of air flow velocities studied. That range yields $\tau \sim O(0.01)$.

We choose to work in a coordinate system moving with the translating mucus block. Thus, with reference to these axes, the mucus is moving with zero velocity in the base state, but the boundary $y = -1$ is now moving with velocity $-\tau/\gamma$. Since we assume that the mucus behaves as a Kelvin–Voigt solid, so that the viscoelastic damping is proportional to the frequency of the deformations, then the damping term δ does not come in at leading order.

The leading-order solution is then

$$\left.\begin{aligned} &u_{s0} = \tau y/\gamma, \quad v_{s0} = 0, \quad U_{m0} = \tau y, \quad V_{m0} = \frac{G_\lambda G y(y-\hat{a})}{2}, \\ &p_{a0} = -\frac{G\hat{a}}{2\gamma}, \quad p_{s0} = \frac{G}{\gamma}\left(\frac{\hat{a}}{2} - R_s y\right). \end{aligned}\right\} \tag{7}$$

In order that linear viscoelasticity be applied, we must assume small deformations in the solid, and thus $\tau, G_\lambda, G \ll 1$. Based on physiological parameters, these terms are small compared to unity, and hence linear elasticity is justified.

3.2. *First-order problem*

The first-order problem for the mucus displacement field (U_{m1}, V_{m1}) is given by

$$G_\lambda \frac{\partial^2 U_{m1}}{\partial t^2} = \frac{\partial^2 U_{m1}}{\partial x^2} + G_\lambda(1 - \mathrm{i}\delta)\frac{\partial^2 U_{m1}}{\partial y^2} + [1 - G_\lambda(1 - \mathrm{i}\delta)]\frac{\partial^2 V_{m1}}{\partial x\,\partial y}. \tag{8}$$

and

$$G_\lambda \frac{\partial^2 V_{m1}}{\partial t^2} = \frac{\partial^2 V_{m1}}{\partial y^2} + G_\lambda(1 - \mathrm{i}\delta)\frac{\partial^2 V_{m1}}{\partial x^2} + [1 - G_\lambda(1 - \mathrm{i}\delta)]\frac{\partial^2 U_{m1}}{\partial x\,\partial y}. \tag{9}$$

The serous layer velocities satisfy

$$\nabla^4 \psi = 0 \quad \text{where} \quad \boldsymbol{u}_{s1} = \nabla \times \psi \boldsymbol{k}, \tag{10}$$

where ψ is the stream function and $\boldsymbol{k}$ is the unit normal in the z-direction. These equations are solved subject to the boundary conditions listed below.

At the air/mucus interface, continuity of normal and tangential stress, as well as the kinematic condition, demand that

$$\left.\begin{aligned} G_\lambda G_{\eta_2} + \frac{\partial V_{m1}}{\partial y} + (1 - 2G_\lambda(1 - \mathrm{i}\delta))\frac{\partial U_{m1}}{\partial x} + \gamma G_\lambda p_{a1} &= \kappa G_\lambda \eta_{2xx} \\ \frac{\partial U_{m1}}{\partial y} + \frac{\partial V_{m1}}{\partial x} &= 0 \\ V_{ml} &= \eta_2. \end{aligned}\right\} \quad \text{at } y = \hat{a}. \tag{11}$$

At the serous/mucus interface we impose, respectively, continuity of normal and tangential stress, the kinematic condition in both the mucus and serous layers, and

continuity of tangential velocity, so that

$$\left.\begin{aligned} G_\lambda G[1-R_s]\eta_2 + \frac{\partial V_{m1}}{\partial y} + (1-2G_\lambda(1-\mathrm{i}\delta))\frac{\partial U_{m1}}{\partial x} &= -\gamma G_\lambda p_{s1} + 2\gamma G_\lambda \frac{\partial v_{s1}}{\partial y} \\ \frac{\partial U_{m1}}{\partial y} + \frac{\partial V_{m1}}{\partial x} &= \frac{\gamma}{(1-\mathrm{i}\delta)}\left[\frac{\partial u_{s1}}{\partial y} + \frac{\partial v_{s1}}{\partial x}\right] \\ V_{m1} &= \eta_1 \\ v_{s1} &= \frac{\partial \eta_1}{\partial t} \\ u_{s1} + \frac{\tau}{\gamma}\eta_1 &= \frac{\partial U_{m1}}{\partial t} \end{aligned}\right\} \text{at } y = 0. \tag{12}$$

Finally, at the airway wall, the no-slip and no-penetration conditions require

$$u_{s1} = v_{s1} = 0 \quad \text{at} \quad y = -1. \tag{13}$$

Note that gravity, G, is included in the normal stress boundary conditions, since the stress from the leading-order state is comparable to that in the first order, even though the strains are small.

Assuming a travelling wave solution so that $U_m \sim f(y)\mathrm{e}^{\mathrm{i}k(x-ct)}$, the general solution for the mucus layer perturbation displacement equations, (8), (9), is then

$$\left.\begin{aligned} U_{m1} &= \left[A_1 \mathrm{i}\frac{\sinh(\alpha k y)}{\alpha} + B_1 \mathrm{i}k\cosh(\alpha k y) + A_2\cosh(\beta k y) + B_2 \beta k \sinh(\beta k y)\right]\mathrm{e}^{\mathrm{i}k(x-ct)}, \\ V_{m1} &= \left[A_1\cosh(\alpha k y) + B_1 \alpha k \sinh(\alpha k y) - \frac{A_2 \mathrm{i}\sinh(\beta k y)}{\beta} - B_2 \mathrm{i}k\cosh(\beta k y)\right]\mathrm{e}^{\mathrm{i}k(x-ct)}, \end{aligned}\right\} \tag{14}$$

where

$$\alpha^2 = 1 - G_\lambda c^2, \quad \beta^2 = 1 - \frac{c^2}{(1-\mathrm{i}\delta)}.$$

In the same way, we assume that the velocity field in the serous layer takes the same form, and hence the solutions to (10) are

$$\left.\begin{aligned} u_{s1} &= [A_3 k\mathrm{e}^{ky} - B_3 k\mathrm{e}^{-ky} + A_4\mathrm{e}^{ky}(1+ky) + B_4\mathrm{e}^{-ky}(1-ky)]\mathrm{e}^{\mathrm{i}k(x-ct)}, \\ v_{s1} &= -\mathrm{i}k[A_3\mathrm{e}^{ky} + B_3\mathrm{e}^{-ky} + A_4 y\mathrm{e}^{ky} + B_4 y\mathrm{e}^{-ky}]\mathrm{e}^{\mathrm{i}k(x-ct)}. \end{aligned}\right\} \tag{15}$$

The disturbance pressure in the serous layer p_{s1} is then

$$p_{s1} = -2\mathrm{i}k[A_4\mathrm{e}^{ky} + B_4\mathrm{e}^{-ky}]\mathrm{e}^{\mathrm{i}k(x-ct)}. \tag{16}$$

Using these forms (14)–(16) and inserting them into the boundary conditions, (11)–(13), leads to ten independent equations for the ten unknown constants. This requires solving the system, $\boldsymbol{A}\boldsymbol{x} = \boldsymbol{0}$ where $\boldsymbol{x}$ is the vector of unknowns, $(A_1, B_1, A_2, B_2, A_3, B_3, A_4, B_4, N_1, N_2)$ with N_1 and N_2 being the amplitudes of the perturbed profiles η_1 and η_2, respectively. If the system is to have non-trivial solutions, then the determinant of $\boldsymbol{A}$ must be zero. This will yield a dispersion relation between the complex wave speed c and the disturbance wavenumber, k. In the limit as $b \to 0$, i.e. $\gamma \to \infty$, the case where there is no fluid and only a viscoelastic solid, with air flow on the top surface,

the dispersion relation recovers that derived in Duncan *et al.* (1985). Since there are infinitely many solution branches, we use asymptotics to determine analytical expressions for c in the long wave limit. We integrate along those branches that are of interest (Im(c) greater than or close to zero) using AUTO (Doedel 1986).

4. Solution branches and wave classification

In the present section we explore the nature of the instabilities of this gas/solid/liquid system in order to gain a deeper understanding of how the presence of the serous layer can affect the stability characteristics of the system. This will be helpful in understanding the results of the following section. In exploring the effect of the serous layer, we need to examine how the stability of the system varies with the serous layer thickness b. Thus, in this section, all lengths are non-dimensionalized with the mucus thickness a, so the dimensionless mucus thickness is unity, and the dimensionless serous layer depth is $\hat{b} = b/a$. Then the dimensionless parameters will have b replaced by a.

The instabilities are determined by solving the dispersion relationship (developed in the previous section) for the complex wave speed c as a function of the wavenumber k. In solving for the group velocity, $\partial(\mathrm{Re}(c)k)/\partial k$, as well as for the phase velocity, Re(c), of the instabilities, we determined that the instabilities were characterized by non-zero group velocity, and hence were convective instabilities, rather than absolute instabilities.

4.1. *Wave classes*

Following the lines of the analysis conducted by Duncan *et al.* (1985) we shall classify the waves in the categories outlined by Landahl and Benjamin, as either class A, B or C waves, depending on the sign of the 'activation energy', ΔE, of the coating. The activation energy is defined as the change in energy of the coating (potential and kinetic) minus the work done by the coating on the flow due to conservative forces only. The system energy is normalized with N_2^2. ΔE is calculated in the same manner as that adopted by Duncan *et al.* (1985), except that we now take into account the conservative work done by the coating on the underlying serous layer, W_s. This work is given by

$$W_s = \frac{k\gamma}{2\,\mathrm{Im}(c)}\mathrm{Re}[(A_4 + B_4)\bar{N}_1\bar{c}]. \tag{17}$$

When ΔE is negative, the work done on the flow is greater than the energy generated in the coating, indicating that there is a net transfer of energy to the flow. These waves are called class A waves, and exhibit the somewhat surprising behaviour that they grow when damping is added to the system. For this reason, class A waves are called damping instabilities. Conversely, when ΔE is positive, there is a net transfer of energy from the flow to the coating, and these waves, called class B waves, decay when damping is added to the system. In class C waves, the work done on the coating is transferred into energy in the coating. Kelvin–Helmholtz instabilities are typical of waves which exhibit class C type behaviour. We shall use these classifications in examining the behaviour of the system due to the presence of the serous layer.

4.2. *Effect of adding the serous layer*

Dispersion relationships for the case of an ideal elastic solid for three different values of serous thickness $\hat{b}$ are shown in figures 2–4, for $\hat{U} = 60$. In studying the different wave classes, we assume that the air viscosity is zero, so that the serous layer is not

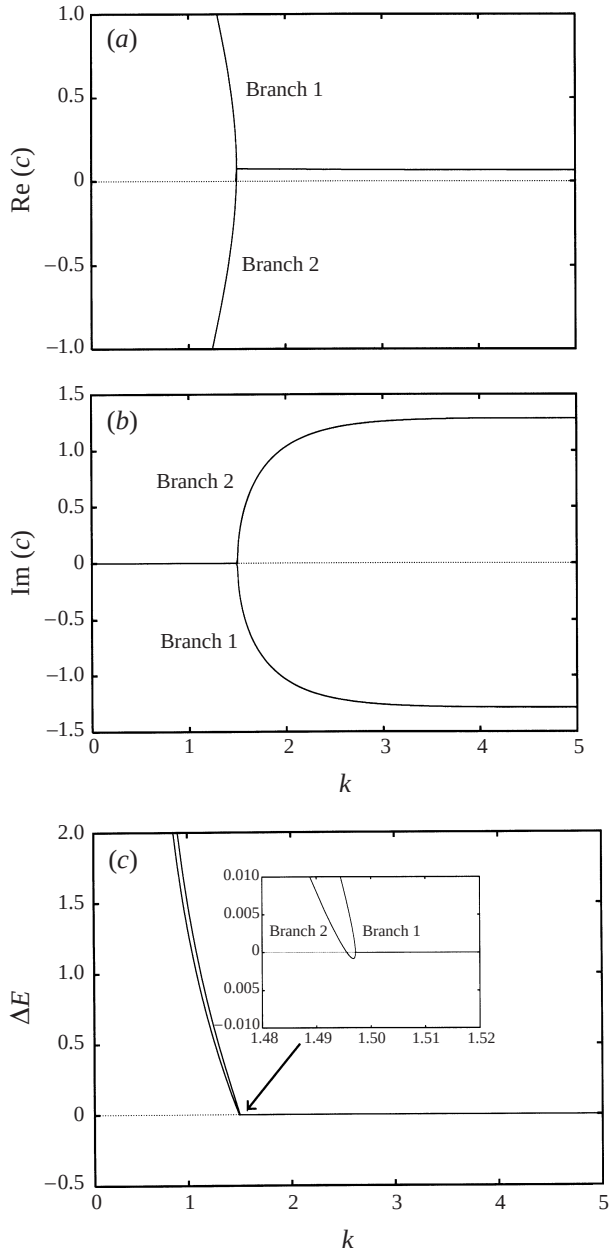

FIGURE 2. (*a*) Wave speed, Re(*c*) vs. *k*; (*b*) growth rate, Im(*c*) vs. *k*; (*c*) activation energy, ΔE vs. *k* for $\hat{b} = 0$ (no serous layer). Remaining parameter values are $\kappa = 0$, $\delta = 0$, $G = 0$, $\gamma = 1$, $G_\lambda = 0.0909$, $R = 0.001$.

moving in the base state, thus ensuring the effect of the serous layer is to always take energy away from the system. We also set gravity, $G = 0$, and surface tension, $\kappa = 0$, so that the focus is solely on the effect of the serous layer. The other parameters have values $R = 0.001$, $R_s = 1$, $\delta = 0$, $\gamma = 1$, $G_\lambda = 0.0909$. Figure 2 shows the wave speed, growth rate and activation energy for the case when $\hat{b}$ is zero, and hence represents the branch of instability described by Duncan *et al.* (1985), but with $R = 0.001$ instead

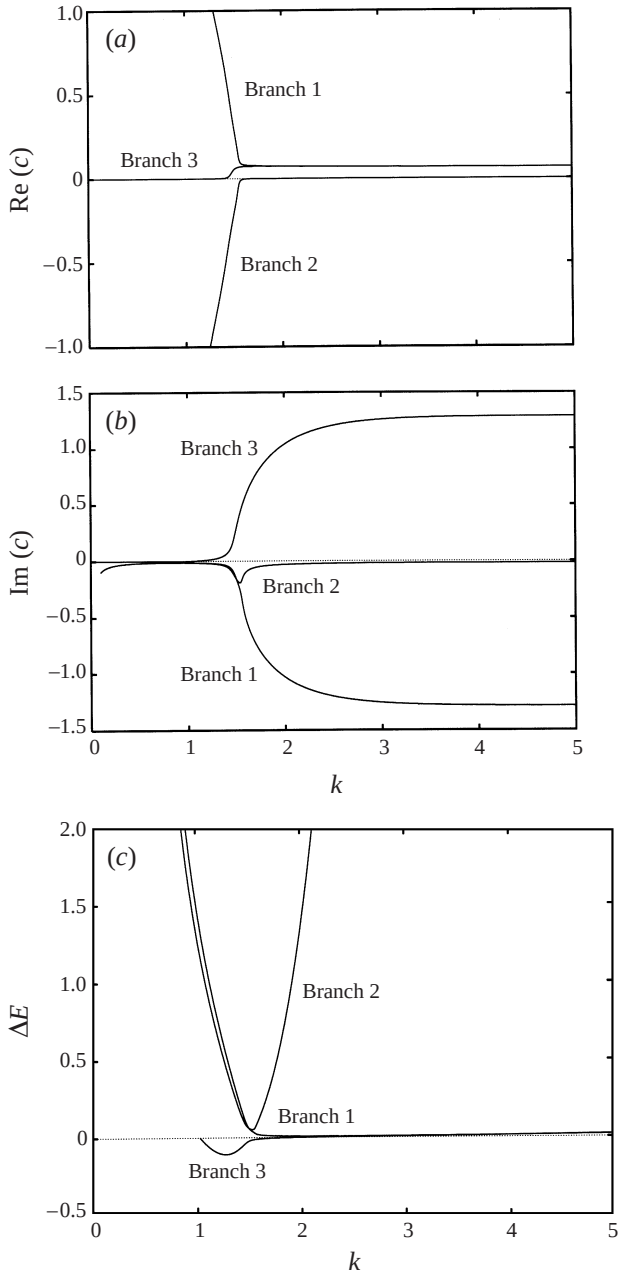

FIGURE 3. (*a*) Wave speed, Re(c) vs. k; (*b*) growth rate, Im(c) vs. k; (*c*) activation energy, ΔE vs. k for $\hat{b} = 0.01$ and $R_s = 1$, remaining parameter values as in figure 2.

of their $R = 1$. In this case, the system is neutrally stable for sufficiently long waves, with waves travelling both upstream and downstream. At some finite value of k the upstream wave begins to travel downstream, and at this point it changes from being a class B wave to a class A wave; the point at which the branch changes wave class is when ΔE becomes negative. At a subsequent wavenumber k, the two waves begin travelling at the same speed, and the system becomes unstable. At this juncture the

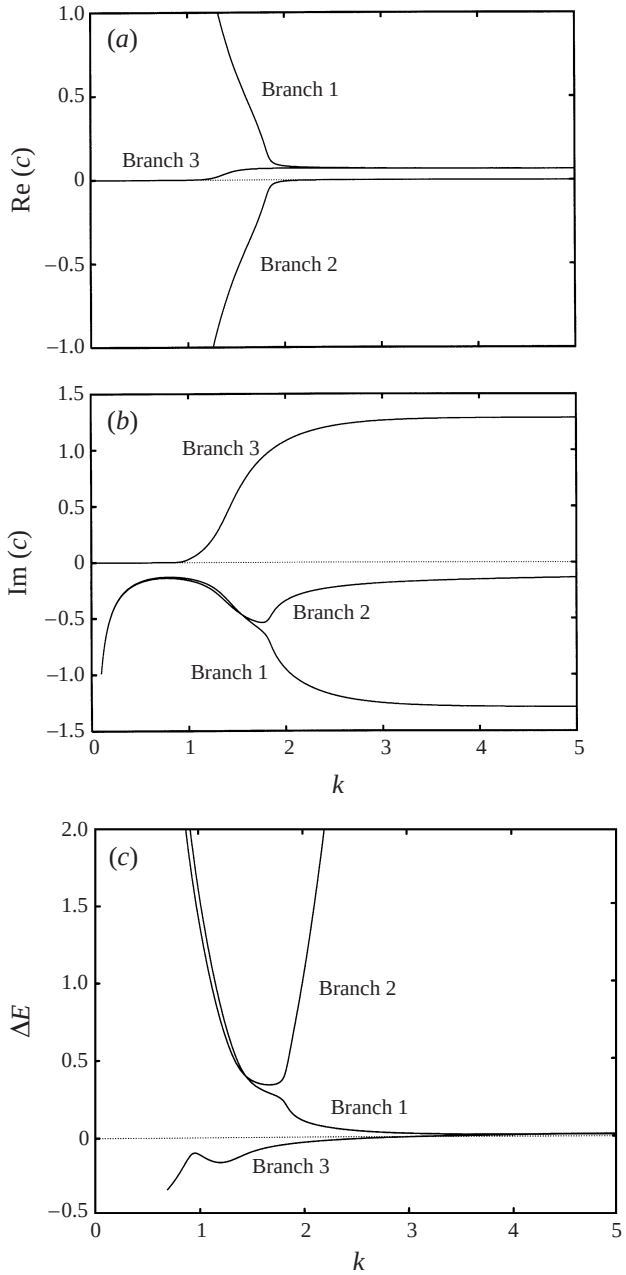

FIGURE 4. (*a*) Wave speed, Re(c) vs. k; (*b*) growth rate, Im(c) vs. k; (*c*) activation energy, ΔE vs. k for $\hat{b} = 0.1$ and remaining parameter values as in figure 3.

two waves possess class C (Kelvin–Helmholtz) characteristics. In the present analysis, the downstream wave is denoted branch 1, and the upstream wave is denoted branch 2. The trivial solution $c = 0$ is also a solution to this system.

As $\hat{b}$ becomes finite, but small, the trivial solution near $k = 0$ splits into two distinct but finite solution branches, branches 3 and 4. The branch 3 solution is shown in figures 3(*a*) and 3(*b*) for $\hat{b} = 0.01$. Note that for shorter waves, away from $k = 0$, the

branch 3 solution actually recovers the upstream (branch 2) solution when $\hat{b} = 0$. In fact, the upstream solution branch (when $\hat{b} = 0$) of Duncan *et al.* (1985) is actually the branch 3 solution when k is large, and the branch 2 solution for k small. The branch 4 solution is not shown, since it does not become important for the range of parameters studied. The corresponding curve for ΔE is shown in figure 3(*c*).

For larger values of $\hat{b}$, branch 3 becomes more distinct, and this is apparent in figures 4(*a*) and 4(*b*) for $\hat{b} = 0.1$. The curve of ΔE vs. k in figure 4(*c*) shows that the class A behaviour of the branch 3 solution extends over a larger range of k.

These wave classification arguments also carry over to systems with a non-zero base state, as well as systems with gravity and surface tension. Since the velocity of the serous layer in the base state is small, the effect on the energy is also small, so that the non-zero base state does not change the wave classification arguments at all. The effect of gravity and surface tension is to increase the energy of the solid by a factor of $G + \kappa k^2$. This accompanying increase in ΔE entails a diminished region of wavenumbers over which class A waves ($\Delta E < 0$) exist; gravity increases the activation energy in a region near $k = 0$, and surface tension increases the energy for large k. Thus, the region of k over which waves grow due to the presence of the viscous sublayer is reduced accordingly.

The long wave instabilities, indicated by $\mathrm{Im}(c) > 0$ in figures 3(*b*) and 4(*b*), are characterized by very small or zero phase speeds. When there is no base-state flow, the phase speed at onset of instability is zero, and the phase speed is only changed by a small amount when there is some finite base-state velocity. This is characteristic of a damping instability.

The asymptotic representation of these four branches in the long wave limit is

$$\left.\begin{aligned} \text{branches 1 and 2: } c &= \pm\frac{1}{\sqrt{RG_\lambda k}} + \hat{U} \mp \frac{\sqrt{RG_\lambda k}}{6R^2 G_\lambda}, \\ \text{branch 3: } c &= \frac{\mathrm{i}\hat{U}^2 R\hat{b}^2 k^2}{12\gamma}, \\ \text{branch 4: } c &= -\frac{4\mathrm{i}\hat{b}k}{\gamma}(1 - G_\lambda). \end{aligned}\right\} \tag{18}$$

Thus, branches 1 and 2 are independent of serous layer properties (to $O(k)$) so that the long-wave behaviour of these two branches is not affected by the presence of the serous layer. These two solutions are the downstream and upstream branches respectively.

Branches 3 and 4 both recover the trivial solution in the limit as $\hat{b} \to 0$. The trivial solution is also a solution to the dispersion relationship derived by Duncan *et al.* (1985). Notice that branch 3 is unstable for all flow speeds, in the long-wave limit, $k \to 0$. In dimensional form, $c = \mathrm{i}\rho_a U_\infty^2 k^2 b^3 / 12\mu_s$, which is independent of all mucus properties, and is thus solely due to the presence of the serous layer. In fact, this instability arises in systems of inviscid air flow over thin viscous layers, with no mucus present (Jeffreys 1924). This instability arises because the air pressure is 180° out of phase with the air/mucus interface. It is important to note here that these asymptotic representations assume that gravity G is zero. If this were not the case, the branch 3 solution, in the small-k limit, would have $c \sim -\mathrm{i}k$, for $G > 0$ and the instability due to the Bernoulli forcing term would become apparent at larger wavenumbers.

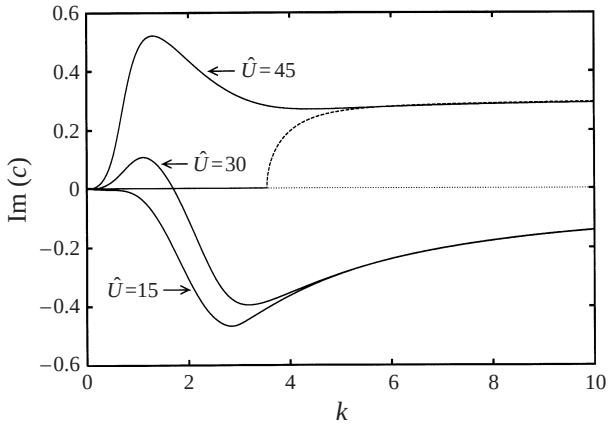

FIGURE 5. Growth rate, Im(c) vs. wavenumber k, for $\hat{U} = 15, 30, 45$, remaining parameter values are $\kappa = 0$, $\delta = 0$, $G = 0.158$, $\gamma = 0.605$, $G_\lambda = 0.0909$, $R = 0.001$, $R_s = 1$, $\hat{a} = 1$. The dashed line is the branch 3 growth rate for $\hat{b} = 0$ and $\hat{U} = 45$.

Below some critical value of $\hat{U}$, given by

$$\hat{U}_0 = \left[\frac{2(1 - G_\lambda)}{R}\right]^{1/2} \tag{19}$$

branch 3 becomes stabilized for shorter wavelengths. Thus, below $\hat{U}_0$, the branch 3 instability becomes apparent only at long wavelengths, and is solely due to the serous layer. Such an instability arises in a system where there is no elastic solid present. Thus, the presence of the elastic solid stabilizes the system for shorter waves, in much the same way that surface tension stabilizes short waves in fluid-only systems. This critical velocity is the same critical velocity derived by Duncan *et al.* (1985) to determine the onset of class A waves. For the values of R and G_λ studied here, $\hat{U}_0 = 42.64$.

When $\hat{U}$ exceeds $\hat{U}_0$, branch 3 represents both the fluid instability at long waves (present when there is no solid) and the solid instability for shorter waves (present when there is no fluid). This effect is demonstrated in figure 5. The solid line is the branch 3 growth rate when $\hat{b} = \hat{a} = 1$. The dashed line is the branch 3 growth rate in the mucus-only limit ($\hat{b} = 0$) and $\hat{U} = 45$ ($> \hat{U}_0$). As can be seen, when $\hat{U} > \hat{U}_0$, and k is sufficiently large, the branch 3 solution recovers the $\hat{b} = 0$ limit.

5. Results

Figures 5–11 are shown for parameter values pertinent to human airways, a list of which is given in table 1. To build our understanding of the full system, we start with the simplest case, of elastic solids ($\delta = 0$) with no surface tension ($\kappa = 0$), and results for this case are shown in figures 5–7.

Figure 5 shows the dispersion relationship relating the disturbance growth rate. Im(c) to the disturbance wavenumber k for various flow speeds, in the elastic limit case ($\delta = 0$). The dashed line is the growth rate for the system with no serous layer, and $\hat{U} = 45$. The solid line is the growth rate for the system with mucus and serous layer thicknesses being equal ($\hat{a} = 1$). The system is always stable for a small range of k near $k = 0$, where it is stabilized by gravity, although this cannot be depicted in

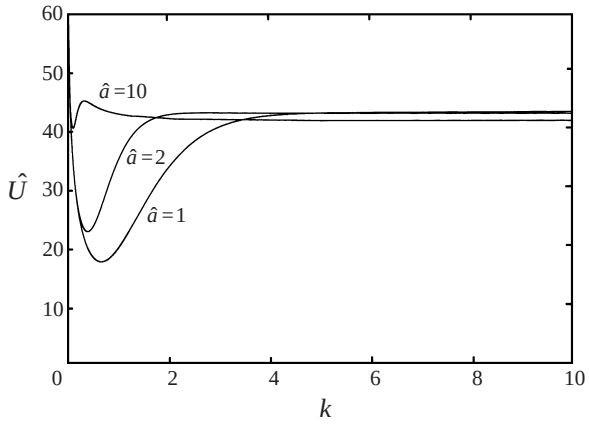

FIGURE 6. Neutral stability curves $\hat{U}$ vs. k for $\hat{a} = 1, 2, 10$, remaining parameter values as in figure 5.

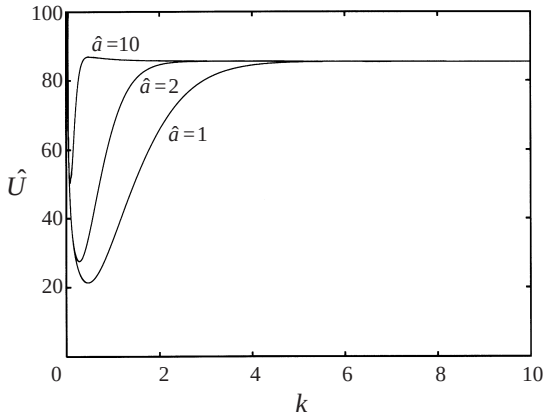

FIGURE 7. Neutral stability curves $\hat{U}$ vs. k for $\hat{a} = 1, 2, 10$, remaining parameter values as in figure 5 except $G_\lambda = 0.3636$.

the figure. When $\hat{U}$ is 15, the system is stable for all k. When $\hat{U} = 30$, it is unstable for a finite range of k; the instability being due to the Bernoulli forcing of the air flow which is transferred directly to the serous layer. The system is stabilized at larger values of k by the presence of the mucus layer, which provides an elastic restoring force to the system, in much the same way surface tension is stabilizing for fluids at shorter wavelengths. When $\hat{U} = 45$, which exceeds the flutter speed (the flow speed required to produce instabilities when there is no serous layer present) the system is unstable for all k, except in the small range of k near zero. The asymptotic result of the previous section for the flutter speed ($\hat{U}_0 = 42.64$) is confirmed here.

Important parameters which change during the course of disease are the mucus shear modulus, G', and the mucus thickness, a. The effects of these two parameters, in the absence of surface tension, are shown in the neutral stability curves of figure 6 and figure 7, where G' of figure 7 is 4 times that in figure 6. Both figures show the air flow velocity at neutral stability, $\hat{U}(\mathrm{Im}(c) = 0)$, plotted vs. the wavenumber, k, for different values of mucus thickness, $\hat{a}$. These curves define the boundary between stability (below the curve) and instability (above). We see that increasing $\hat{a}$ raises the neutral stability curves to higher speeds. We might expect this since a thicker

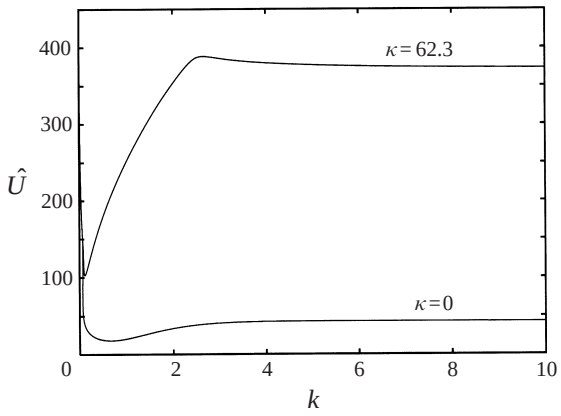

FIGURE 8. Neutral stability curves for $\kappa = 0, 62.3$, remaining parameter values as in figure 5.

elastic slab has a larger bending stiffness which tends to stabilize the system and also shift the local minima to smaller values of k, longer waves. The destabilizing effect of the serous layer reduces to zero in the limit $\hat{a} \gg 1$. It is evident from both figures that the critical flow speed, $\hat{U}_c$, to precipitate the instability (the minimum of the neutral stability curve) is significantly less than that which would be obtained in the mucus-only system. This observation agrees qualitatively with the experimental studies of air flowing over a mucus simulant (mayonnaise) lying on top of a thin, oily sublayer (Basser *et al.* 1989).

Figure 8 shows the neutral stability curve for two different values of the surface tension parameter, κ with $\hat{a} = 1$. Notice that surface tension raises the air velocity required to initiate instability. The critical air velocity, $\hat{U}_c$, is shown in figure 9(*a*) as a function of mucus thickness, $\hat{a}$. Two choices are shown for the dimensional surface tension values: $\sigma = 0$ dyn cm^{-1} ($\kappa = 0$) and $\sigma = 10$ dyn cm^{-1} ($\kappa = 62.3$). Surface tension provides a stabilizing force to the system, especially for shorter waves. In fact, when $\sigma = 10$ dyn cm^{-1}, the flutter instability due to the coupling of the air flow and the solid material, which occurs at shorter wavelengths, is stabilized; the only instability is a damping instability arising from the presence of the serous layer. It is this damping instability which defines onset, and since surface tension also provides a stabilizing mechanism to the fluid, it can significantly delay onset. This effect is illustrated in figure 9(*a*), which shows increased $\hat{U}_c$ for finite surface tension. For the case when there is finite surface tension at the mucus/air interface, the dependence of onset flow speed on mucus thickness that we saw in figures 6 and 7 is, in fact, reversed. The neutral stability curves for dimensionless surface tension, $\kappa = 0$ and $\kappa = 62.3$ are shown in figure 8. As can be seen, finite surface tension significantly increases the critical air velocity for large k. This is because surface tension is stabilizing when k is large.

A similar reversal is seen in figure 9(*b*) where $\hat{U}_c$ is plotted as a function of mucus stiffness for two different values of κ. When $\kappa = 0$, the onset flow speed increases as the mucus stiffness increases, consistent with the comparison of figure 6 to figure 7. Increasing the mucus stiffness is thus stabilizing in this system. However, when the surface tension is non-zero, as depicted in the curve for $\kappa = 62.3$, the onset flow speed decreases as the stiffness increases. The basis of these two interesting reversals is discussed below.

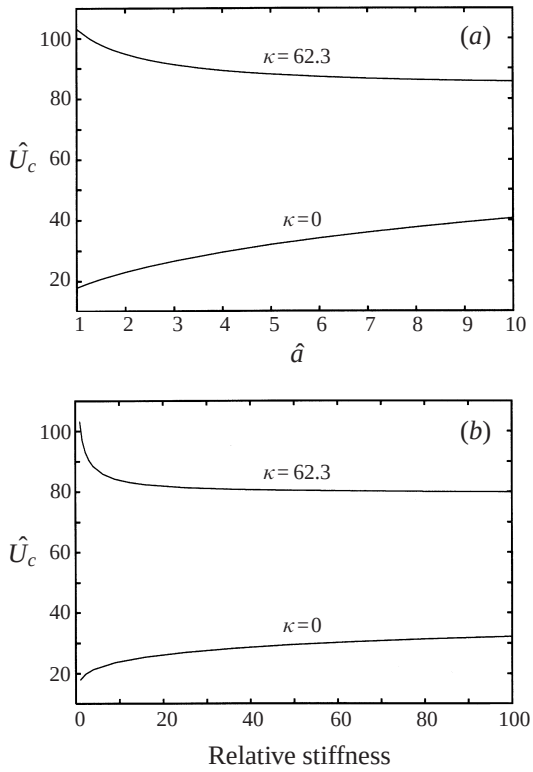

FIGURE 9. (*a*) Onset stability curve $\hat{U}_c$ vs. $\hat{a}$; and (*b*) vs. relative shear modulus, for $\kappa = 0, 62.3$, remaining parameter values as in figure 5.

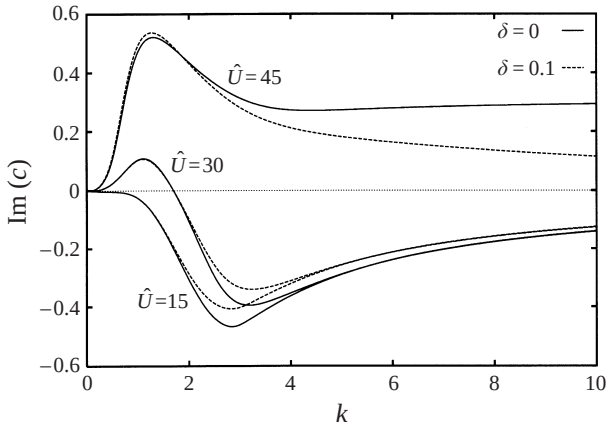

FIGURE 10. Growth rate Im(c) vs. k showing the effect of mucus damping, $\delta = 0, 0.1$ and remaining parameter values as in figure 5.

Figure 10 shows the effect of mucus damping on growth rates. The material damping only affects the system at larger wavenumbers where the flutter instability is the dominant mode of instability. The effect of material damping is to cause the short-wave flutter instabilities to decay. Hence, for sufficient damping the class C waves actually exhibit class B behaviour in this parameter range. The effect of

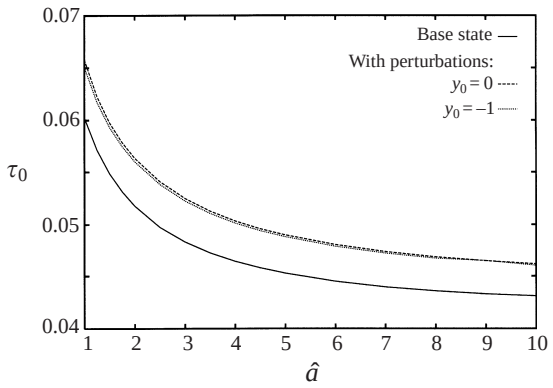

FIGURE 11. Dimensionless shear stress at onset, $\tau_0 = \gamma\, \partial u/\partial y$ at $y = y_0$ vs. $\hat{a}$ for $\kappa = 62.3$. The remaining parameter values are as in figure 5.

material damping at shorter wavelengths is to enhance growth, which is as expected, since the waves are class A waves in this regime. Material damping has a very small effect, $O(k^3)$, on the long-wavelength instabilities, i.e. in the limit $k \to 0$, so that the flow speeds at onset are not significantly affected by the viscous nature of the material. This is because it is the serous layer which determines onset velocities, and thus mucus damping has little effect on the system at onset. The shear stresses at the mucus/serous interface ($y = 0$) and at the wall ($y = -1$) are shown in figure 11 and indicate that they are well below the mucus yield stress ($\tau = 20$), thus validating our assumption that the mucus can be modelled as a viscoelastic solid during travelling wave disturbances.

6. Discussion

The results indicate that air flow velocities required to precipitate instabilities for a mucus–serous bilayer are approximately $5.0\,\mathrm{m\,s^{-1}}$ ($\sim 100C_t$), when the surface tension of the air–mucus interface is $\sigma = 10\ \mathrm{dyn\,cm^{-1}}$. Higher values of σ may be found in the lung airway (Schurch *et al.* 1990), as mentioned earlier, and the resulting stiffer system would increase the critical air speed. The air flow velocities required to initiate waves on the air–mayonnaise surface ($\sigma = 9\ \mathrm{dyn\,cm^{-1}}$) in the experiments of Basser *et al.* (1989) fell in the range 10–$30\,\mathrm{m\,s^{-1}}$($\sim$ (100–300)C_t), so our theoretical predictions are close to their critical velocity data. In terms of disturbance wavelengths at the onset of instability, only one or two undulations on the surface of the mayonnaise were observed in Basser *et al.* (1989), so it is difficult to match theory and experiment. Also, the growth is very rapid and large-deformation nonlinear analysis would be required. However, long wavelengths at onset, approximately five times the mucus thickness, would agree with the results of our theory.

The serous sublayer significantly modifies the mechanical system, according to our theory. In contrast to theories of air flow over a single, elastic layer (Duncan *et al.* 1985 and Evrensel *et al.* 1993), the base condition of our bilayer system is a viscoelastic slab in uniform motion, dragged over a thin viscous film and parallel to the rigid plane underneath. Because of its much larger viscosity, the perturbation stresses in this liquid film are large compared to the air flow perturbations at criticality. So the film becomes an important contributor to the resulting mechanics. The experiments in Basser *et al.* (1989) included ones where the choice of

channel bottom material had an effect on the critical flow speed. When polyethylene was used, the critical speeds were approximately half the value of those where a cheesecloth bottom was used. Viscometric studies, using a cone–plate apparatus, showed that an oily, sublayer film developed between the mayonnaise and polyethylene. Unlike our model, this film was non-Newtonian, since the viscometric studies indicate a system yield stress between 75 to 150 dyn cm^{-2} with no yield of the mayonnaise layer. Once this yield stress of the film is exceeded in an air flow experiment, and there is viscous flow in the sublayer, the polyethylene system is Basser *et al.* (1989) is similar to our theory and, presumably, the physiological setting where the serous sublayer (Newtonian) is present. Our theory predicts faster growth rates for the wave instability in the presence of this thin, viscous-behaving film. This may contribute to the observed decrease in stability with a polyethylene undersurface, attributed to the decreased yield stress in the avalanche theory.

Basser *et al.* (1989) found that increasing θ from 0.4 to 0.9 lead to an increase in critical air velocity when the cheesecloth was used at the mayonnaise/channel interface. Since the oily sublayer was not deposited for a cheesecloth bottom, the solid boundary conditions are similar to the theory of Evrensel *et al.* (1993) who predicted that critical speeds decrease with thicker mucus layers, an opposite result. The reason for the prediction by Evrensel *et al.* (1993), that a decrease in critical air velocity occurs with increasing mucus thickness, is that they assume a constant flow rate of air through the channel. Smaller cross-sectional areas therefore entail larger flow velocities leading to larger shear stresses and smaller critical flow velocities. Our theory predicts that thicker mucus layers, larger $\hat{a}$, raise the critical air velocity for $\sigma = 0$ and lower it for $\sigma = 10$ dyn cm^{-2}. The effect of surface tension, apparently, is to reverse the parametric dependence of critical velocity on mucus thickness. Surface tension effects were discussed in the theory of Basser *et al.* (1989) who concluded that it is not important in their experiments, using an analogy to wind–water waves. The difficulty with this approach is that the wind–water wave model used assumes an inviscid, deep fluid, not a non-Newtonian material with a yield stress and a shallow depth.

Our theory predicts surface tension to be a significant factor in the physiological system. We are uniquely positioned to comment here, since our model takes the novel step of including surface tension on the air boundary of a viscoelastic slab. The ratio $\kappa' = (\sigma/dG')$ is the important dimensionless parameter which measures the relative significance of surface tension forces and elastic shear forces. This parameter may be viewed as the ratio of a length scale, $L = \sigma/G'$, which measures the distance over which surface tension at the air/mucus interface is felt through the mucus, to a physical thickness, d, which may be taken as characteristic for the bi-layer. When $d = b$, the sublayer thickness, this ratio is our parameter κ. We saw a reversal of the influence of a (figure 9*a*) and relative stiffness (figure 9*b*) depending on the surface tension, which is large for the pulmonary application ($\kappa \sim 180$). For a system with no sublayer, one could choose $d = a$, the slab thickness. Inserting the mayonnaise parameter values, where the slab thicknesses b are on the order 0.2 cm, $\kappa' \sim 0.5$. So surface tension effects are not dominant in Basser *et al.* (1989); however, according to our analysis this would be on the basis of the mayonnaise slab thicknesses being large compared to the physiological values of mucus thickness, $a \sim 0.001$ to 0.01 cm. Our approach is consistent with the thesis of an avalanche cascade, however, because the avalanche is precipitated by the onset of a surface wave, the mechanisms of which we examine in a bilayer, air–solid–liquid interaction.

7. Conclusions

We have developed a mathematical model to simulate and explore the fundamental nature of the instabilities which develop when air flows over a viscoelastic material lying on top of a viscous sublayer. The motivation behind this work is to study mucus clearance in the lung, although the model could also be used to study other systems, such as the removal of ice on airplane wings during flight. In the case of ice, the transverse elastic wave speed is approximately 10^5 times larger than that of mucus (Ashby & Jones 1980), so that the dominant instability over all realistic wavenumbers is the flutter instability.

In order to understand the instability regimes, we have calculated the activation energy of the solid, so that we can classify the waves and hence interpret the wave behaviour when fluid and material damping is added to the system. This has involved calculating the strain and kinetic energies of the elastic solid, as well the work done on the air flow and viscous sublayer by the solid. We have seen that the presence of the serous layer can give rise to long-wavelength instabilities, which are class A waves, so that they grow with viscous damping. The presence of the viscous sublayer has little or no effect on shorter waves where the instability is predominantly a flutter instability set up between the air flow and the solid medium.

The long-wave instabilities are due to the Bernoulli forcing of the air flow, and would arise in systems where there is no mucus layer present. For shorter waves, when the flow speed is less than $[2(1-G_\lambda)/R]^{1/2}$, and there is no surface tension, the system can become stabilized; in this regime the solid supplies an elastic restoring force to the system, in much the same way that surface tension can stabilize fluids at shorter wavelengths. When $\hat{U} > [2(1-G_\lambda)/R]^{1/2}$, the system recovers the flutter instability for shorter waves.

We have included the effect of surface tension at the air/mucus interface, not a feature of previous theories. The new dimensionless surface tension parameter, κ, is the ratio of surface tension to elastic shear forces so $\kappa \gg 1$ implies a system dominated by surface tension and $\kappa \ll 1$ implies a system dominated by the stiffness of the mucus. In general, surface tension stiffens the entire system, but its value can reverse the effect of mucus thickness on critical velocities. Surface tension also acts to stabilize flutter instabilities at larger wavenumbers, so that the instability of the system at onset is entirely due to the presence of the serous layer. Our results show that the air flow speed required to precipitate instabilities is much lower than that required in systems where there is no serous layer. This agrees qualitatively with the observations made in the experiments of Basser *et al.* (1989) at onset, in the small deformation regime.

A caveat to these theories and experiments is that during a cough, air flow velocities can be very large, as mentioned earlier. The instabilities discussed in the present work and that of Basser *et al.* (1989) occur at much smaller air velocities. Therefore, neither mechanism may be directly responsible for mucus clearance during a cough, since other effects may supersede: airway wall movement, transient inertial effects, turbulent bursts. The wall motion, for example, may be a partial collapse of the airway followed by wall flutter as studied in Grotberg & Shee (1985), Grotberg & Reiss (1984), Grotberg & Gavriely (1989), Gavriely *et al.* (1989) and LaRose & Grotberg (1997). Additionally, an important consideration for the role of the bilayer is not only how the serous fluid may assist in clearance of the mucus, but also how both layers may protect the underlying airway epithelial cells from excessive fluid shear forces.

This work was supported by NSF grant CTS 9412523, NASA grants NAG3-1959 & NAG3-2196 and The Whitaker Foundation.

REFERENCES

Ashby, M. F. & Jones, D. R. H. 1980 *Engineering Materials*. Pergamon.

Basser, P. J., McMahon, T. A. & Griffith, P. 1989 The mechanism of mucus clearance in cough. *J. Biomech. Engng* **111**, 288–297.

Benjamin, T. B. 1963 The threefold classification for unstable disturbances in flexible surfaces bounding inviscid flows. *J. Fluid Mech.* **16**, 436–450.

Clarke, S. W., Jones, J. G. & Oliver, D. R. 1970 Resistance to two-phase gas-liquid flow in airways. *J. Appl. Physiol.* **29**, 464–471.

Davis, S. S. 1973 Rheological examination of sputum and saliva and the effect of drugs. In *Rheology of Biological Systems*, pp. 157–194. Charles C. Thomas.

Doedel, E. 1986 AUTO: *Software for Continuation and Bifurcation Problems in Ordinary Differential Equations*. Concordia University, Montreal, Quebec, Canada.

Dulfano, M. J., Adler, K. & Philippoff, W. 1971 Sputum viscoelasticity in chronic bronchitis. *Am. Rev. Respir. Dis.* **104**, 88–98.

Duncan, J. H., Waxman, A. M. & Tulin, M. P. 1985 The dynamics of waves at the interface between a viscoelastic coating and a fluid flow. *J. Fluid Mech.* **158**, 177–197.

Evrensel, C. A., Khan, R. U., Elli, S. & Krumpe, P. E. 1993 Viscous airflow through a rigid tube with a compliant coating: a simple model for the air mucus interaction in pulmonary airways. *J. Biomech. Engng* **115**, 262–270.

Gavriely, N., Shee, T. R., Cugell, D. W. & Grotberg, J. B. 1989 Flutter in flow-limited collapsible tubes: a mechanism for generation of wheezes. *J. Appl. Physiol.* **66**, 2251–2261.

Grotberg, J. B. 1994 Pulmonary flow and transport phenomena. *Ann. Rev. Fluid Mech.* **26**, 529–571.

Grotberg, J. B. & Gavriely, N. 1989 Flutter in collapsible tubes: a theoretical model of wheezes. *J. Appl. Physiol.* **66**, 2262–2273.

Grotberg, J. B. & Reiss, E. L. 1984 Subsonic flapping flutter. *J. Sound Vib.* **92**, 349–361.

Grotberg, J. B. & Shee, T. R. 1985 Compressible-flow channel flutter. *J. Fluid Mech.* **159**, 175–193.

Jeffreys, H. 1924 On the formation of water waves by wind. *Proc. R. Soc. Lond.* A **107**, 189–206.

King, M., Brock, G. & Lundell, C. 1985 Clearance of mucus by simulated cough. *J. Appl. Physiol.* **58**, 1776–1782.

King, M., Chang, H. K. & Weber, M. E. 1982 Resistance of mucus lined tubes to steady and oscillatory airflow. *J. Appl. Physiol.* **52**, 1172–1176.

King, M. & Macklem, P. T. 1977 Rheological properties of microliter quantities of normal mucus. *J. Appl. Physiol.* **42**, 797–802.

Landahl, M. T. 1962 On the stability of a laminar incompressible boundary layer over a flexible surface. *J. Fluid Mech.* **13**, 607–632.

LaRose, P. G. & Grotberg, J. B. 1997 Flutter and long wave instabilities in compliant channels conveying developing flows. *J. Fluid Mech.* **331**, 37–58.

Powell, R. L., Aharonson, E. F., Schwarz, W. H., Proctor, D. F., Adams, G. K. & Reasor, M. 1974 Rheological behavior of normal tracheobronchial mucus of canines. *J. Appl. Physiol.* **37**, 447–451.

Riley, J. J., Gad-el-Hak, M. & Metcalfe, R. W. 1988 Compliant coatings. *Ann. Rev. Fluid Mech.* **20**, 393–420.

Ross, B. B., Gramiak, R. & Rahn, H. 1955 Physical dynamics of the cough mechanism. *J. Appl. Physiol.* **8**, 264–269.

Scherer, P. W. & Burtz, L. 1978 Fluid mechanical experiments relevant to coughing. *J. Biomech.* **11**, 183–187.

Schlichting, H. 1979 *Boundary Layer Theory*. McGraw-Hill.

Schurch, S., Gehr, P., Im Hof, V., Geiser, M. & Green, F. 1990 Surfactant displaces particles toward the epithelium in airways and alveoli. *Respir. Physiol.* **80**, 17–32.

Shah, P. L., Scott, S. F., Knight, R. A., Marriott, C., Ranasinha, C. & Hodson, M. E. 1996 In vivo effects of recombinant human DNase I on sputum in patients with cystic fibrosis. *Thorax* **51**, 119–125.

Sleigh, M. A., Blake, J. R. & Liron, N. 1988 The propulsion of mucus by cilia. *Am. Rev. Respir. Dis.* **137**, 726–741.

Suki, B., Pedersen, O. F., Habib, R. & Jackson, A. C. 1995 Wave speed during maximal expiratory flow and phase velocity from forced oscillations. *Respir. Physiol.* **102**, 39–49.

Wu, R. & Carlson, D. M. 1991 Structure and synthesis of mucins. In *The Lung: Scientific Foundations*, vol. 1, pp. 183–188. Raven Press, Ltd.